
PERGAMON

Journal of Quantitative Spectroscopy & Radiative Transfer 79–80 (2003) 953–972

Journal of Quantitative Spectroscopy & Radiative Transfer

www.elsevier.com/locate/jqsrt

Aerosol retrievals from AVHRR radiances: effects of particle nonsphericity and absorption and an updated long-term global climatology of aerosol properties

Michael I. Mishchenko[a,*], Igor V. Geogdzhayev[a,b], Li Liu[a,c], John A. Ogren[d], Andrew A. Lacis[a], William B. Rossow[a], Joop W. Hovenier[e,f], Hester Volten[f,g], Olga Muñoz[h]

[a] *NASA Goddard Institute for Space Studies, 2880 Broadway, New York, NY 10025, USA*
[b] *Department of Applied Physics and Applied Mathematics, Columbia University, 2880 Broadway, New York, NY 10025, USA*
[c] *Department of Earth and Environmental Sciences, Columbia University, 2880 Broadway, New York, NY 10025, USA*
[d] *Climate Monitoring and Diagnostics Laboratory, NOAA, 325 Broadway R/CMDL1, Boulder, CO 80305, USA*
[e] *Department of Physics and Astronomy, Free University, De Boelelaan 1081, 1081 HV Amsterdam, The Netherlands*
[f] *Astronomical Institute "Anton Pannekoek," University of Amsterdam, Kruislaan 403, 1098 SJ Amsterdam, The Netherlands*
[g] *FOM-Institute for Atomic and Molecular Physics, Kruislaan 407, 1098 SJ Amsterdam, The Netherlands*
[h] *Instituto de Astrofisica de Andalucia, P.O. Box 3004, Granada 18080, Spain*

Received 24 May 2002; accepted 18 August 2002

Abstract

The paper describes and discusses long-term global retrievals of aerosol properties from channel-1 and -2 Advanced Very High-Resolution Radiometer (AVHRR) radiances. We reconfirm the previously reached conclusion that the nonsphericity of dust-like and dry sea salt aerosols can lead to very large errors in the retrieved optical thickness if one mistakenly applies the scattering model for spherical particles. Comparisons of single-scattering albedo and Ångström exponent values retrieved from the AVHRR data and those measured in situ at Sable Island indicate that the currently adopted value 0.003 can be a reasonable choice for the imaginary part of the aerosol refractive index in the global satellite retrievals. Several unexpected features in the long-term satellite record indicate a serious problem with post-launch calibration of channel-2 radiances from the NOAA-11 spacecraft. We solve this problem by using a simple re-calibration procedure removing the observed artifacts and derive a global climatology of aerosol optical thickness and size over the oceans

* Corresponding author. Tel.: +1-212-678-5590; fax: +1-212-678-5622.
E-mail address: crmim@giss.nasa.gov (M.I. Mishchenko).

0022-4073/03/$ - see front matter
doi:10.1016/S0022-4073(02)00331-X

for the period extending from July 1983 to December 1999. The global monthly mean optical thickness and Ångström exponent of tropospheric aerosols show no significant trends over the entire period and oscillate around the average values 0.145 and 0.75, respectively. The Northern Hemisphere mean optical thickness systematically exceeds that averaged over the Southern Hemisphere. The AVHRR retrieval results during the period affected by the Mt. Pinatubo eruption are consistent with the retrievals of the stratospheric aerosol optical thickness based on Stratospheric Aerosol and Gas Experiment data (SAGE). Time series of the aerosol optical thickness and Ångström exponent derived for four separate geographic regions exhibit varying degrees of seasonal variability controlled by local meteorological events and/or anthropogenic activities.

Keywords: Atmospheric aerosols; Nonspherical particles; Remote sensing

1. Introduction

The important role of tropospheric aerosols in forming the Earth's climate is now well recognized [1–3] and has motivated several dedicated research programs [4–6], including the Global Aerosol Climatology Project (GACP) established in 1998 as part of the National Aeronautics and Space Administration's Radiation Sciences Program and the World Climate Research Programme's Global Energy and Water Cycle Experiment [7]. A major component of the GACP is a retrospective analysis of the Advanced Very High-Resolution Radiometer (AVHRR) radiance data set in order to infer the long-term global distribution of aerosols, their properties, and seasonal and interannual variations.

In recent publications [8,9], we described an advanced aerosol retrieval algorithm based on using channel-1 and -2 AVHRR data over the oceans and applied it to the ISCCP DX radiance dataset [10]. Specifically, the algorithm retrieves the aerosol optical thickness τ and Ångström exponent A for each pixel by minimizing the difference between two radiances measured in the 0.65 and 0.85 μm channels at the specific illumination and observation angles determined by the satellite orbit on the one hand and the radiances computed theoretically for a realistic atmosphere–ocean model on the other hand. The Ångström exponent is defined as

$$A = -\left.\frac{\mathrm{d}[\ln C_{\mathrm{ext}}(\lambda)]}{\mathrm{d}(\ln \lambda)}\right|_{\lambda=\lambda_1}, \tag{1}$$

where $\lambda_1 = 0.65$ μm is the nominal wavelength of the AVHRR channel 1 and C_{ext} is the ensemble-averaged extinction cross-section per particle. With only two pieces of data per pixel available, one can retrieve only the two model parameters and must assign fixed global values to the remaining parameters describing the complex atmosphere–ocean system, thereby introducing potential biases in the aerosol product. We have performed an extensive study of the expected accuracy of the algorithm and its sensitivity to various a priori assumptions and used it in the development of a preliminary global climatology of the aerosol optical thickness and size for the period extending from July 1983 to August 1994.

This paper is a logical continuation of [8,9] and has four major objectives. First, it is well known that the climatically important dust-like aerosols have nonspherical shapes, whereas the operational GACP algorithm is based on Lorenz-Mie computations and assumes the spherical particle shape

irrespective of aerosol type. It is, therefore, important to examine how nonsphericity can affect the results of AVHRR aerosol retrievals. This will be the subject of the following section.

Second, the inherent limitations of a retrieval algorithm based on utilizing only two pieces of data per pixel [8,9] force one to adopt a spatially and temporally fixed value of the imaginary part of the aerosol refractive index. The current version of the algorithm [9] uses the value 0.003, which is smaller than the value 0.005 used in the initial version [8], the reason being that this decrease may help to achieve a better balance between the nonabsorbing sea salt aerosols and the absorbing anthropogenic and dust aerosols on a global scale. Although the effect of this change on the retrieved optical thickness and Ångström exponent was found to be relatively small, one can expect a more significant effect on the retrieved single-scattering albedo. The latter is not a formal operational product, but follows implicitly from the retrieved Ångström exponent and the assumed shape of the aerosol size distribution and the real and imaginary parts of the aerosol refractive index. The availability of extensive in situ measurements of the single-scattering albedo at Sable Island as reported by Delene and Ogren [11] enable us to examine the accuracy of our choice of the imaginary part of the refractive index, at least in the Atlantic Ocean area adjacent to that location. This will be done in Section 3.

Third, our previous analysis [9] revealed a discontinuity in the retrieved Ångström exponent at the time of NOAA-9 to NOAA-11 spacecraft transition and significant temporal trends in the global optical thickness and Ångström exponent values not consistent with the properties of aerosols from the Mt. Pinatubo eruption. Since the AVHRR instrument does not include an on-board radiance calibrator for the solar wavelength channels, these results were interpreted as an indication of a serious calibration problem. Section 4 will be devoted to a more detailed analysis of this issue and will describe a feasible approach to solving the calibration problem based on reasonable assumptions about the temporal variability of the global aerosol load and size.

Finally, in Section 5 we will apply the two-channel retrieval algorithm to the re-calibrated AVHRR radiances and derive a global climatology of aerosol optical thickness and size over the oceans for the period extending from July 1983 to December 1999. We will also analyze and discuss temporal trends in the global and regional aerosol characteristics.

2. Effect of particle shape

Desert dust can dominate the aerosol population over large Atlantic Ocean areas off the north-west coast of Africa, the Persian Gulf region, and large areas of the Pacific Ocean off the coast of China. Sea salt particles are believed to be the dominant aerosol species at high southern latitudes. It has been demonstrated recently that particle nonsphericity is an important factor that must be carefully addressed in optical characterization of mineral aerosols such as dust-like and dry sea salt particles [12–15]. Previous analyses of this issue were based either on semi-empirical approximate approaches [16,17] or on theoretical computations of the phase function for simplified model shapes [13–15,18–21]. However, theoretical and numerical techniques are still limited in their ability to simulate electromagnetic scattering by realistic polydispersions of irregular particles. Therefore, laboratory measurement techniques [22,23] remain an important source of information on scattering properties of natural nonspherical aerosols.

Recently, Volten et al. [24,25] presented an extensive dataset which includes the results of laboratory measurements for several types of polydisperse, randomly oriented mineral aerosols at 441.6 and 632.8 nm wavelengths. A limitation of these measurements is the lack of data at very small and very large scattering angles (from 0° to 5° and from 173° to 180°), which precludes the determination of the absolute angular dependence of the phase function $a_1(\Theta)$ by using the standard normalization condition,

$$\frac{1}{2}\int_0^\pi d\Theta \sin\Theta\, a_1(\Theta) = 1, \tag{2}$$

where Θ is the scattering angle. As a consequence, Volten et al. plotted the relative quantity $\tilde{a}_1(\Theta) = a_1(\Theta)/a_1(30^\circ)$ rather than $a_1(\Theta)$, which limits the applicability of their results in satellite remote sensing. However, Liu et al. [26] used the relative angular profile of the phase function measured by Volten et al. [24,25] for a quartz particle sample at 441.6 nm to construct a synthetic phase function on the entire interval $\Theta \in [0^\circ, 180^\circ]$ by assuming that the forward-scattering diffraction peak is independent of the particle shape and depends only on the distribution of surface-equivalent-sphere radii and the wavelength, and then using the normalization condition (2). The quartz phase function was selected because the refractive index of quartz is rather well known in the visible spectral range. Furthermore, the experimental angular profile of the phase function for the quartz sample appeared to be only weakly dependent on the wavelength and was similar to those of the other mineral aerosol samples studied by Volten et al. irrespective of their exact size distribution and chemical composition.

Since the synthetic phase function is available only for one average particle size relative to the wavelength, it cannot be used in the operational two-channel algorithm in order to retrieve simultaneously the aerosol optical thickness and size. However, it can be used in a one-channel algorithm analogous to that used by Stowe et al. [27], wherein the average particle size (and, thus, the phase function) is assumed to be fixed globally and the only retrieved parameter is τ. Although this approach does not generate a product similar to that based on the two-channel algorithm [8,9], it allows us to study, at least semi-quantitatively, the potential effect of nonsphericity on the aerosol optical thickness retrieved from the AVHRR data. This follows, indeed, from the theoretical observation that the spherical–nonspherical differences in the phase function should be very similar for the two close AVHRR channels [19].

Volten et al. [24,25] defined the equivalent-sphere radius r of a nonspherical particle as the radius of a sphere that has a projected area equal to the average projected area of the nonspherical particle in random orientation. The effective radius $r_{\rm eff}$ and effective variance $v_{\rm eff}$ [28] of the quartz particle sample studied in [24,25] are 2.3 and 2.4 μm, respectively. The laboratory measurements were performed at a wavelength of 441.6 nm. Therefore, the effective radius of a phase-function-equivalent size distribution at the AVHRR channel-1 wavelength 650 nm is 3.39 μm, thereby representing the coarse mode of dust-like aerosols. The extrapolation of the results obtained at 441.6 nm to 650 nm is based on the assumption that the refractive index of quartz remains nearly constant in this spectral interval, which is indeed the case.

Fig. 1 depicts the synthetic phase function as well as the phase function for projected-area-equivalent quartz spheres calculated using the Lorenz-Mie code described in [29] and available on-line at http://www.giss.nasa.gov/∼crmim. In close agreement with previous results of Jaggard et al. [30] for Raft River soil dust and the results of theoretical studies of light scattering by

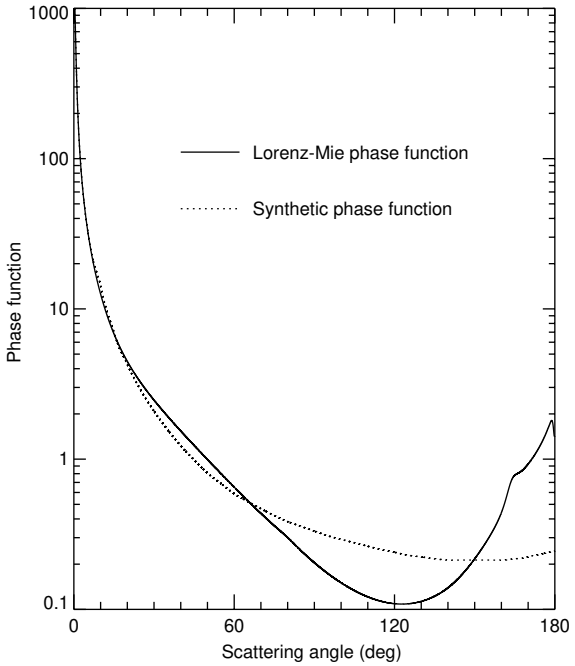

Fig. 1. Synthetic and Lorenz-Mie phase functions for nonspherical quartz aerosols and projected-area-equivalent quartz spheres, respectively, used in the one-channel retrieval algorithm (see text).

polydisperse, randomly oriented spheroids and circular cylinders [19,31], Fig. 1 exhibits the following three conspicuous regions:

$$\begin{aligned} &\text{nonsphere} < \text{sphere} \quad \text{from } \Theta \sim 15^\circ\text{–}20^\circ \text{ to } \Theta \sim 65^\circ, \\ &\text{nonsphere} \gg \text{sphere} \quad \text{from } \Theta \sim 65^\circ \text{ to } \Theta \sim 150^\circ, \\ &\text{nonsphere} \ll \text{sphere} \quad \text{from } \Theta \sim 150^\circ \text{ to } \Theta = 180^\circ. \end{aligned} \tag{3}$$

The differences between the Lorenz-Mie and the synthetic phase function are quite significant at side-scattering angles, where they can exceed a factor of two, and are even greater at backscattering angles.

We have used both phase functions in the one-channel retrieval algorithm and applied the latter to AVHRR data collected in 1987 over a region often dominated by Sahara dust aerosols and extending from the Central Meridian to 60°W and from 7°S to 18°N. We then calculated the monthly average of the ratio of the aerosol optical thickness τ_N retrieved with the phase function of the nonspherical quartz particles to the optical thickness τ_S retrieved with the phase function computed for the projected-area-equivalent spherical quartz aerosols at $\lambda = 0.65$ μm. This ratio is plotted in Fig. 2 as a function of longitude for 1°-wide horizontal belts along with the corresponding monthly averages of the scattering angle.

Fig. 2 is an excellent illustration of the relationships summarized by Eq. (3) and shows that $\tau_N/\tau_S > 1$ for $\Theta > 150^\circ$ and $\tau_N/\tau_S < 1$ for $\Theta < 150^\circ$. Owing to the specific NOAA-9 spacecraft

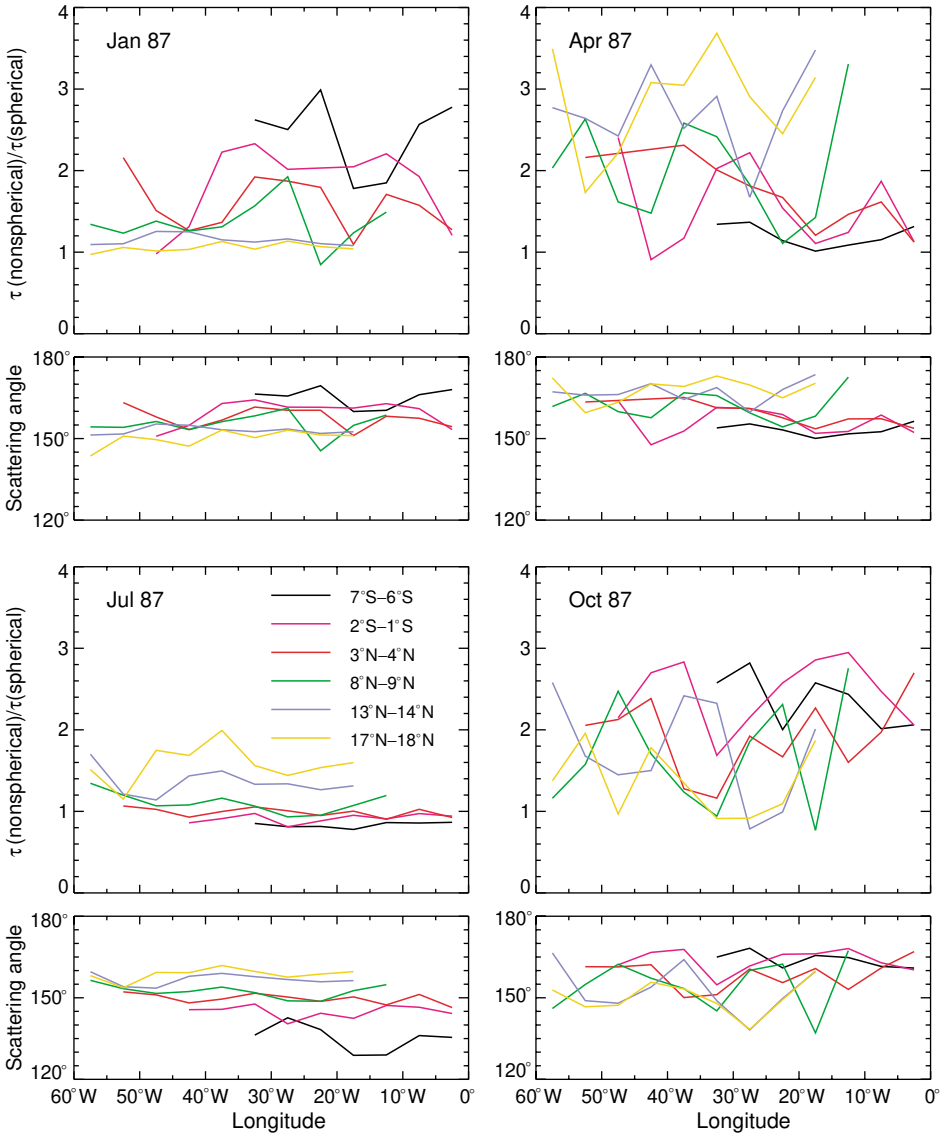

Fig. 2. Monthly averages of the ratio τ_N/τ_S and the respective scattering angle versus longitude.

orbit, the scattering angle for this area is, for the most part, greater than 150° during the four months studied. As a consequence, the algorithm based on the Lorenz-Mie phase function tends to generate significantly smaller optical thicknesses than that based on the phase function representative of nonspherical aerosols. The ratio τ_N/τ_S reaches values exceeding 3.5 in April, but stays closer to unity in July. Accordingly, the monthly averages of this ratio over the entire area studied are 1.545 for January, 1.975 for April, 1.053 for July, and 1.974 for October.

Our results obviously reinforce the previously reached conclusion [18] that the nonsphericity of mineral particles can have a profound effect on the reflected intensity and must be explicitly ac-

counted for in aerosol retrievals based on satellite radiance data. Unfortunately, the AVHRR data by themselves provide no means of identifying particle type and shape. This is also true for any instrument taking reflectance data at only one scattering geometry per pixel, such as the MODerate resolution Imaging Spectrometer (MODIS) [32,33]. Although small values of the Ångström exponent can be indicative of the presence of large mineral particles, this test cannot be expected to distinguish between dry (nonspherical) and wet (spherical) sea salt particles. It thus appears to be difficult, if not impossible, to develop a simple and reliable procedure which improves the AVHRR retrieval algorithm by introducing the necessary corrections when the particles happen to be nonspherical. However, this may be feasible with multi-angle instruments such as the Multiangle Imaging Spectro-Radiometer (MISR) [13,34], the POLarization and Directionality of Earth Reflectances (POLDER) instrument [35,36], and the Earth Observing Scanning Photopolarimeter [37], especially when polarization of the reflected light is also measured.

3. Effect of absorption

Although the aerosol single-scattering albedo ϖ is not included explicitly in the operational product generated by the two-channel retrieval algorithm [8,9], it can be determined from the implicit relationship between ϖ and the Ångström exponent provided that the aerosol refractive index m is fixed. Fig. 3 shows this relationship computed using the Lorenz-Mie theory for $\mathrm{Re}(m)=1.5$ and four increasing values of $\mathrm{Im}(m)$. As in [8,9], we use the simple power law distribution of aerosol radii

$$n(r,\alpha)=\begin{cases} C(\alpha), & r\leqslant r_1,\\ C(\alpha)\left(\dfrac{r}{r_1}\right)^{-\alpha}, & r_1<r\leqslant r_2,\\ 0, & r>r_2 \end{cases} \tag{4}$$

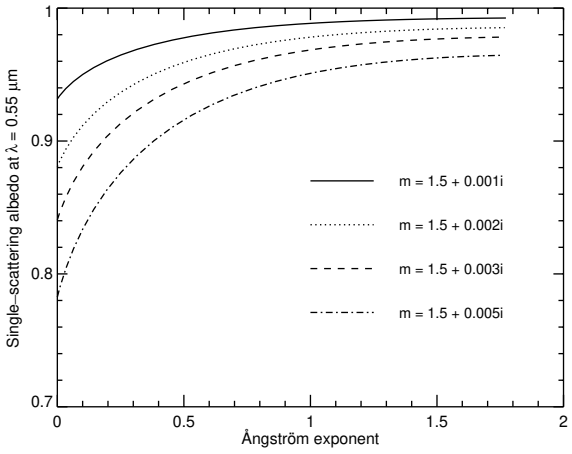

Fig. 3. Aerosol single-scattering albedo versus Ångström exponent for $\mathrm{Re}(m)=1.5$ and four increasing values of $\mathrm{Im}(m)$.

with $r_1 = 0.1$ μm, $r_2 = 10$ μm, and $\alpha \in [2.5, 5]$, where the normalization constant $C(\alpha)$ is chosen such that

$$\int_0^\infty \mathrm{d}r\, n(r, \alpha) = 1. \tag{5}$$

Obviously, the $\varpi(A)$ dependence is always monotonic, and ϖ always decreases with particle size. Furthermore, ϖ always decreases with increasing Im(m).

The current version of the two-channel algorithm uses the value Im(m)=0.003 [9]. Fig. 4 illustrates the single-scattering albedo for July 1999 (lower panel) determined from the retrieved constrained Ångström exponent (upper panel). The latter means that only the Ångström exponent values falling in the interval (0.05, 1.72) are retained [9]. It is seen that ϖ varies from 0.86 to 0.98 and is indeed smaller in areas dominated by larger particles. Unfortunately, this implicit relationship can be unphysical in that it does not allow large but weakly absorbing particles (e.g., sea salt aerosols) to have greater single-scattering albedos than smaller but strongly absorbing particles (e.g., soot aerosols). However, the choice of a constant Im(m) can still be optimized in such a way that it provides a realistic global average value of the single-scattering albedo. Although the latter is not known at present, the extensive in situ measurements of ϖ at Sable Island (43.933°N, 60.007°W) reported by Delene and Ogren [11] can be used to validate our choice of Im(m), at least for that region of the Atlantic Ocean.

The measurements by Delene and Ogren cover the period from 23 November 1994 to 15 April 2000 and are summarized in Fig. 5. For comparison, Fig. 5 also depicts the results of AVHRR retrievals averaged over a 100×100 km square centered at Sable Island for the period from November 1994 to December 1999. It is seen that the in situ single-scattering results may be best reproduced by an Im(m) value between 0.002 and 0.003. Figs. 6 and 7 show a rather weak dependence of the retrieved aerosol optical thickness and Ångström exponent on Im(m) for Im(m) in the range [0.002, 0.003] and suggests that the current choice Im(m) = 0.003 is quite consistent, at least for locations in the vicinity of Sable Island. This conclusion is only reinforced by the inspection of Table 1, which suggests that an Im(m) value close to 0.0025 is needed to reproduce the long-term mean in situ value of the single-scattering albedo and a value close to 0.0035 could reproduce the long-term mean in situ value of the Ångström exponent [11].

4. Calibration

In a previous publication [9], Geogdzhayev et al. presented a preliminary climatology of the aerosol optical thickness and Ångström exponent covering the period from July 1983 to August 1994 based on AVHRR data from the NOAA-7, -9, and -11 satellites and noticed a potential radiance calibration problem with the AVHRR instrument on the NOAA-11 spacecraft. Here we add retrievals from NOAA-14 to the previous record, thereby extending the temporal coverage through December 1999, and suggest a way to compensate for the NOAA-11 calibration problem.

As previously, our aerosol retrievals for the period of NOAA-14 observations were based on the well-established ISCCP post-launch calibration of channel-1 radiances [10]. On the other hand, a significant uncertainty exists in the values of the post-launch calibration coefficients for channel-2 radiances [38]. We, therefore, decided to use the pre-launch channel-2 calibration coefficients for the

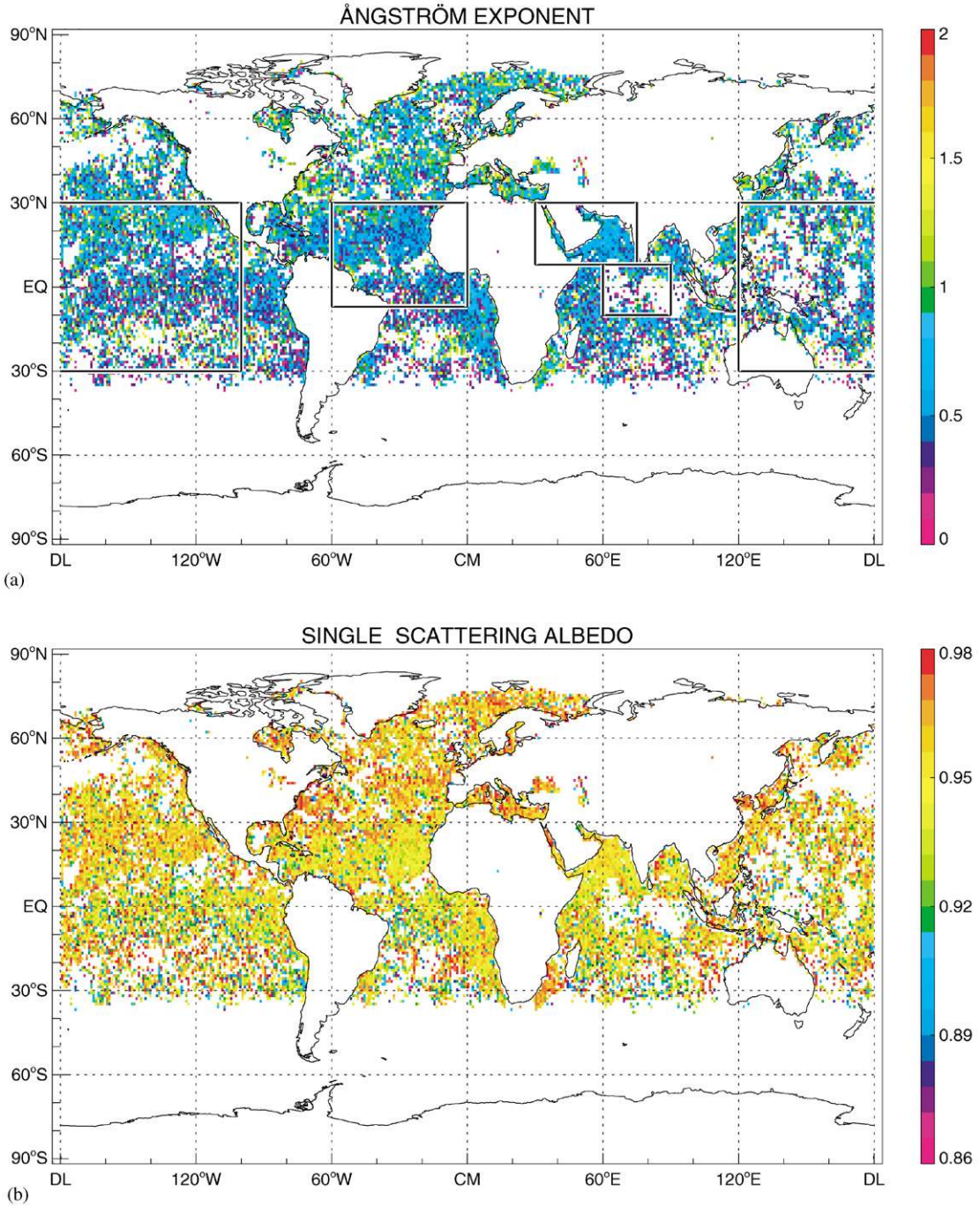

Fig. 4. Monthly averages of the Ångström exponent and single-scattering albedo for July 1999 derived from two-channel AVHRR data assuming a fixed aerosol refractive index $m = 1.5 + 0.003i$.

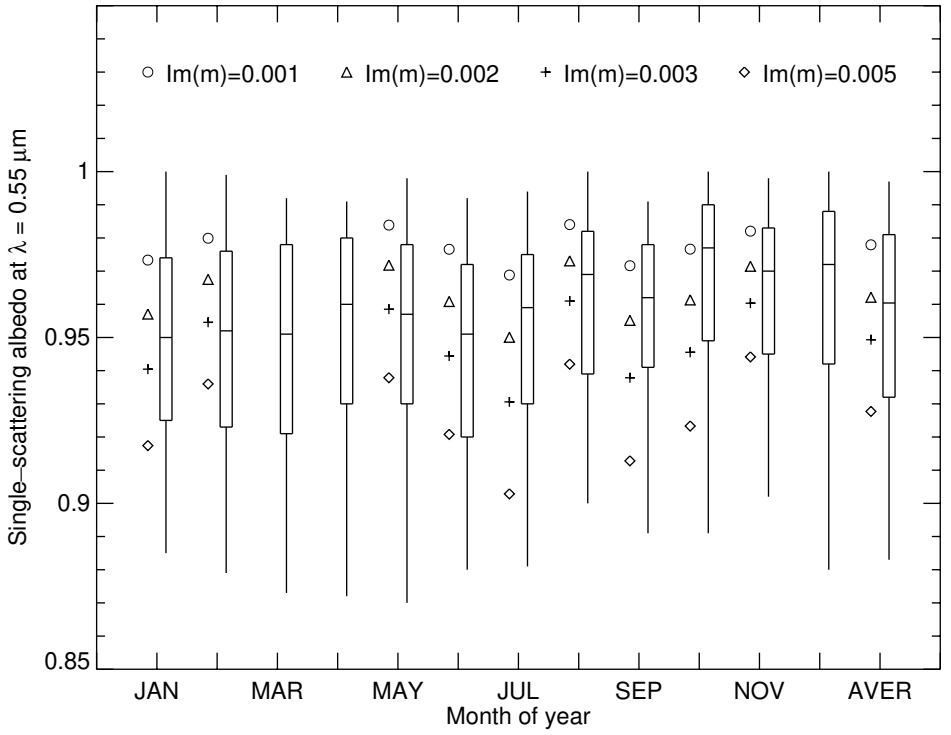

Fig. 5. The annual cycle of the aerosol single-scattering albedo measured in situ at Sable Island [11]. The whiskers denote the 5 and 95 percentiles, the bottom and top of the box denote the 25 and 75 percentiles, and the horizontal line within the box denotes the median value. The statistics are based on the hourly averaged data for all valid measurements obtained during the period 11/23/1994–04/15/2000. The horizontal axis shows the month of year, with the last tick mark representing the statistics for the entire study period. The circle, triangle, plus, and diamond signs represent the average monthly ϖ values retrieved from channel-1 and -2 AVHRR data during the period 11/1994–12/1999 assuming that the imaginary part of the aerosol refractive index is fixed at 0.001, 0.002, 0.003, and 0.005, respectively. The AVHRR results for March, April, and December were not computed because of the insufficient number of cloud-free pixels during these months.

NOAA-14 data while still using the post-launch calibration coefficients for the NOAA-7, -9, and -11 channel-2 radiances [39].

Panels (a) and (b) of Fig. 8 show time series of the global monthly mean aerosol optical thickness and Ångström exponent, respectively, for a 10-year period from 1987 to 1997, which includes the entire NOAA-11 lifetime (November 1988–August 1994). One can clearly see a pronounced discontinuity in the retrieved Ångström exponent at the time of NOAA-9 to NOAA-11 transition (November 1988) and a strong linear downward trend during the NOAA-11 lifetime depicted by the straight red line in Fig. 8(b). Unfortunately, there is a gap between the time when the NOAA-11 spacecraft finished the operation (August 1994) and the time when data from NOAA-14 became available (February 1995). Moreover, the NOAA-11 data became scarce and unreliable after January 1994 as the satellite was nearing the end of its lifetime and its orbit drifted so much that essentially no coverage was available for the Southern Hemisphere. The analysis of the NOAA-11 optical thickness record was further complicated by the Mt. Pinatubo eruption in June of 1991. However,

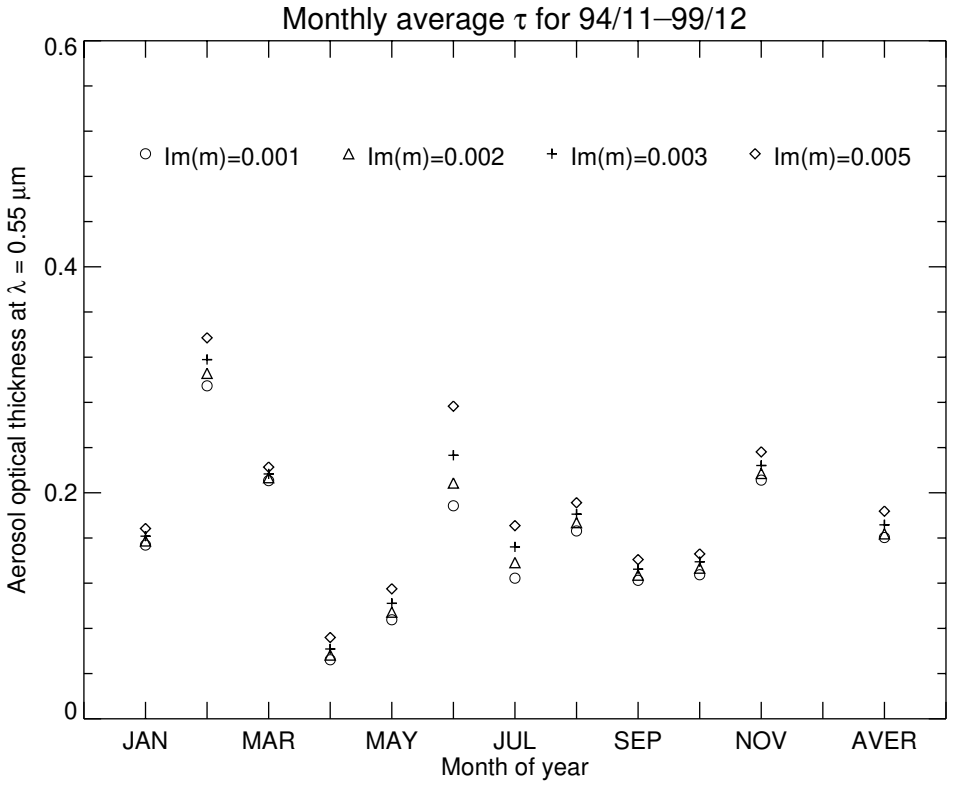

Fig. 6. The annual cycle of the aerosol optical thickness retrieved from channel-1 and -2 AVHRR data over Sable Island during the period November 1994–December 1999 assuming that the imaginary part of the aerosol refractive index is fixed at 0.001, 0.002, 0.003, and 0.005. The horizontal axis shows the month of year, with the last tick mark representing the average results for the entire study period. The AVHRR results for December were not computed because of the insufficient number of cloud-free pixels.

a simple subtraction of the global monthly average of the stratospheric aerosol optical thickness [40,41] from the AVHRR retrieval results also reveals a significant linear trend (the straight red line in panel (a)) in what can be considered a proxy to the tropospheric aerosol optical thickness during the period of Mt. Pinatubo eruption (the yellow curve). This optical thickness trend is consistent with the Ångström exponent trend and clearly indicates a calibration problem with the channel-2 NOAA-11 radiances.

As discussed in [9], aerosol retrievals over the dark ocean surface are most sensitive to the assumed deep space count (or offset) values. The latter are difficult to determine accurately, which leads to significant differences between the results reported by different groups. In order to compensate for the obviously artificial trends in the NOAA-11 retrievals, which are not consistent with the results from other NOAA satellites and the expected effect of the Mt. Pinatubo eruption, we have modified the channel-2 offset values by adding a component which decreases linearly from 0.003 in November 1988 to −0.003 in August 1994. The revised NOAA-11 retrievals are shown in panels (c) and (d) of Fig. 8. Now one can see no significant trend in either the Ångström exponent or the

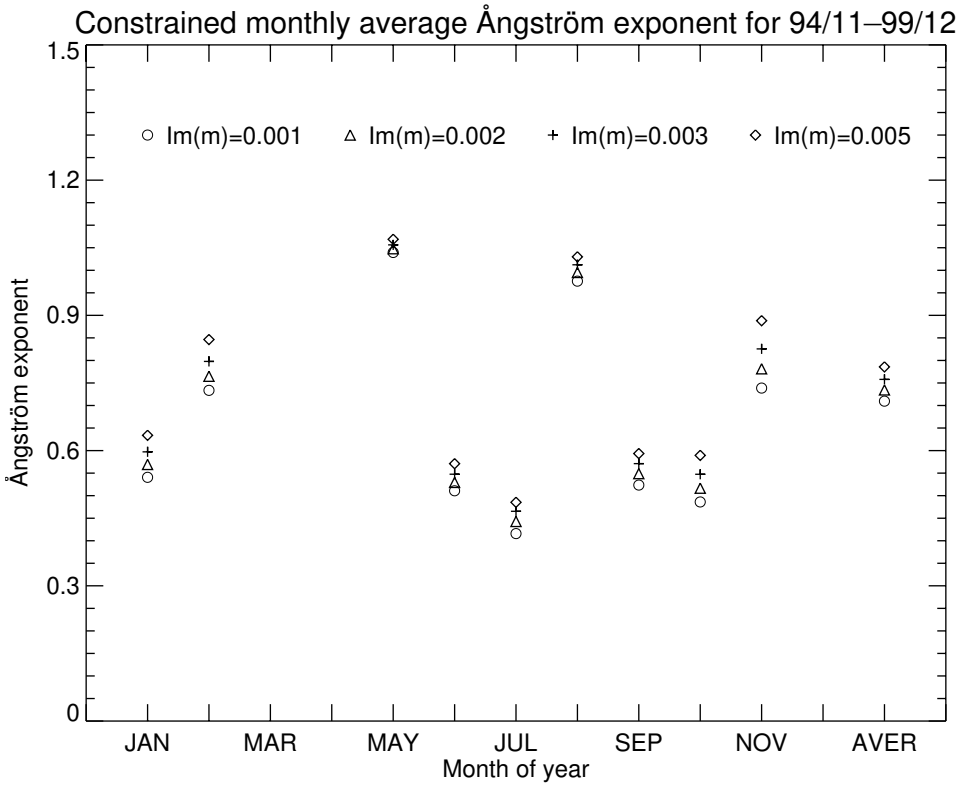

Fig. 7. As in Fig. 6, but for the constrained Ångström exponent. The AVHRR results for March, April, and December were not computed because of the insufficient number of cloud-free pixels during these months.

Table 1
Mean values of aerosol parameters retrieved from AVHRR data and measured in situ at Sable Island

Im(m)	ϖ	τ	A
	Retrieved values for 11/1994–12/1999		
0.001	0.978	0.160	0.710
0.002	0.962	0.164	0.735
0.003	0.949	0.172	0.758
0.005	0.928	0.184	0.786
	In situ values for 11/1994–04/2000 [11]		
	0.956	—	0.770

"tropospheric" τ (yellow curve in panel (c)). Furthermore, the NOAA-11 results are now more consistent with the NOAA-9 and NOAA-14 retrievals. The fact that the adjustment of only one variable (the channel-2 offset) improved the retrieval of both the aerosol optical thickness and the Ångström

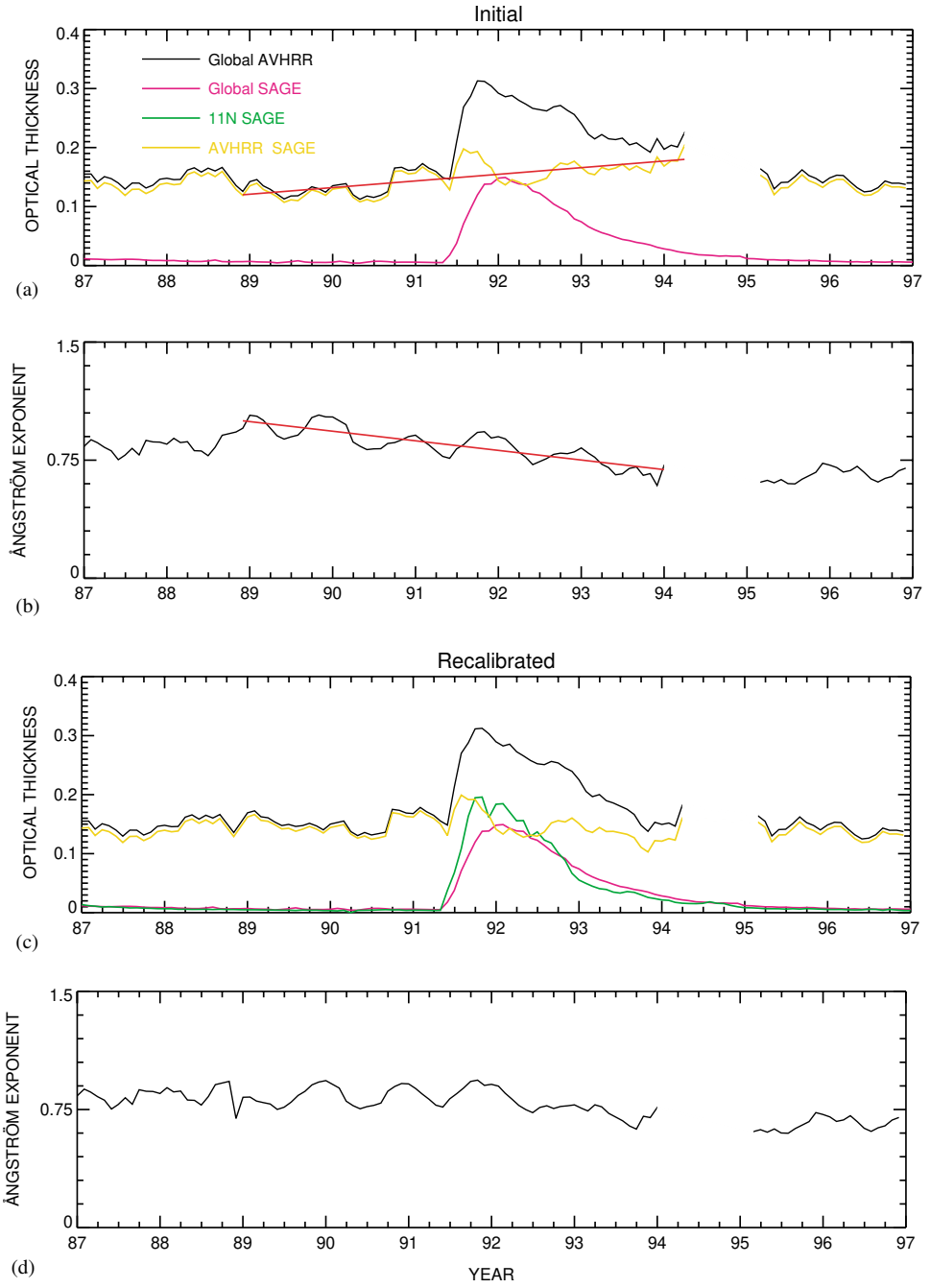

Fig. 8. The time series of the monthly global mean aerosol optical thickness and Ångström exponent retrieved from the AVHRR data and the monthly global mean optical thickness of stratospheric aerosols retrieved from the Stratospheric Aerosol and Gas Experiment (SAGE) data (see text).

exponent is an additional, although indirect, indication of the soundness of our re-calibration procedure.

5. Updated aerosol climatology

Fig. 9 shows updated composite time series of global and hemispheric monthly mean aerosol optical thickness and Ångström exponent based on AVHRR data from the NOAA-7, -9, -11, and -14 satellites covering the period from July 1983 to December 1999. The resulting product is posted on the world wide web at http://gacp.giss.nasa.gov/retrievals. Also shown is the global stratospheric aerosol optical thickness based on Stratospheric Aerosol and Gas Experiment (SAGE) measurements [40,41].

The extended aerosol record shows no obvious long-term trend in the global mean optical thickness of tropospheric aerosols between the periods of major volcanic eruptions. This appears to provide a strong indication that there are no significant flaws in the radiance calibration used. Furthermore, since the drift of the NOAA satellite orbits caused significant changes in the time of observation at a particular point and, thus, in the illumination geometry over the period studied, the absence of a pronounced long-term trend may also indicate that the accuracy of the surface bidirectional reflectance modeling was sufficiently good and that the two-channel algorithm did a reasonably good job in terms of introducing no systematic bias in the aerosol retrievals.

The upper panel of Fig. 9 suggests that the average aerosol load tends to be greater in the Northern than in the Southern Hemisphere and that there is an annual variability pattern in the global average of the optical thickness with maxima occurring around January–February and minima in June–July. The Northern Hemisphere exhibits a similar pattern, but with maxima in February–April. One can clearly discern the residual effect of the El Chichon eruption (March 1982) in the form of increased optical thickness values in the beginning of the record. The June 1991 eruption of Mt. Pinatubo resulted in a sharp increase in the optical thickness to more than double its normal value. The temporal behavior of the constrained Ångström exponent (lower panel of Fig. 9) exhibits less regularity than that of the optical thickness. There seems to be a weak downward trend over the period studied, but it remains unclear whether it is real or is an artifact of residual radiance calibration drifts. The long-term mean aerosol optical thickness values obtained by averaging over the periods not affected by major volcanic eruptions are 0.145 for the entire globe, 0.161 for the Northern Hemisphere, and 0.133 for the Southern Hemisphere. The respective Ångström exponent values are 0.75, 0.78, and 0.73.

One can notice that the maximum of the global average aerosol optical thickness caused by the Mt. Pinatubo eruption occurs at slightly different times in the AVHRR and SAGE global records (see the upper panel of Fig. 9). This can be explained by differences in the geographic coverage provided by the two instruments. Indeed, the SAGE instrument provides measurements over both the continents and the oceans, whereas the AVHRR retrievals are only available over the oceans. Furthermore, the AVHRR coverage is in the form of a latitudinal belt, which varies with season and causes a large fraction of the retrievals to occur at latitudes between 60°S and 60°N, whereas the SAGE coverage extends significantly farther toward the poles. Since it took several months for the volcanic particles to spread by the atmospheric circulation from the equatorial region to the poles, the maximum in τ occurred earlier in the AVHRR than in the SAGE global record. This is illustrated

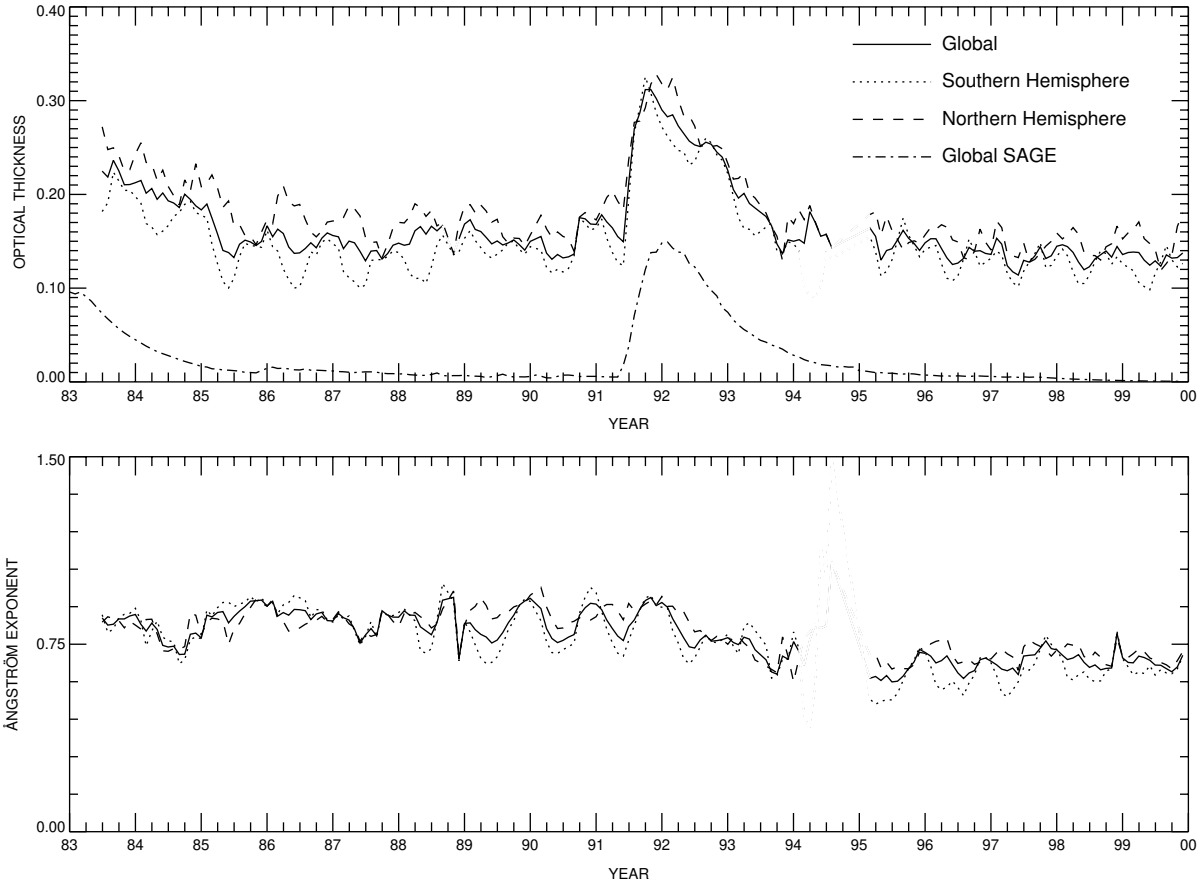

Fig. 9. Time series of monthly mean aerosol optical thickness and Ångström exponent retrieved from AVHRR and SAGE data (see text).

by the 11°N latitudinal mean SAGE aerosol retrieval (green curve in Fig. 8(c)), which shows an optical thickness maximum at exactly the same time as the global AVHRR record.

To study regional trends in the retrieved aerosol properties, we calculated separate time series for the following four geographic regions: (i) a large area of the Pacific Ocean extending from 100°W to 120°E and from 30°S to 30°N; (ii) a tropical Atlantic Ocean area extending from the Central Meridian to 60°W and from 7°S to 30°N; (iii) a Persian Gulf area extending from 30°E to 75°E and from 8°N to 30°N; and (iv) an adjacent part of the Indian Ocean extending from 60°E to 90°E and from 10°S to 8°N (see the upper panel of Fig. 4). As one can conclude from the results shown in Figs. 10 and 11, the large Pacific Ocean area exhibits the weakest seasonal variability of optical thickness, perhaps lightly modulated by biomass burning events in South America and Asia and industrial pollution in China. The optical thickness time series for the Atlantic Ocean area off the west coast of Africa reveals significantly higher aerosol amounts and a much more pronounced seasonality controlled by strong Sahara dust outflows. The average Ångström exponent values for these two regions are rather similar.

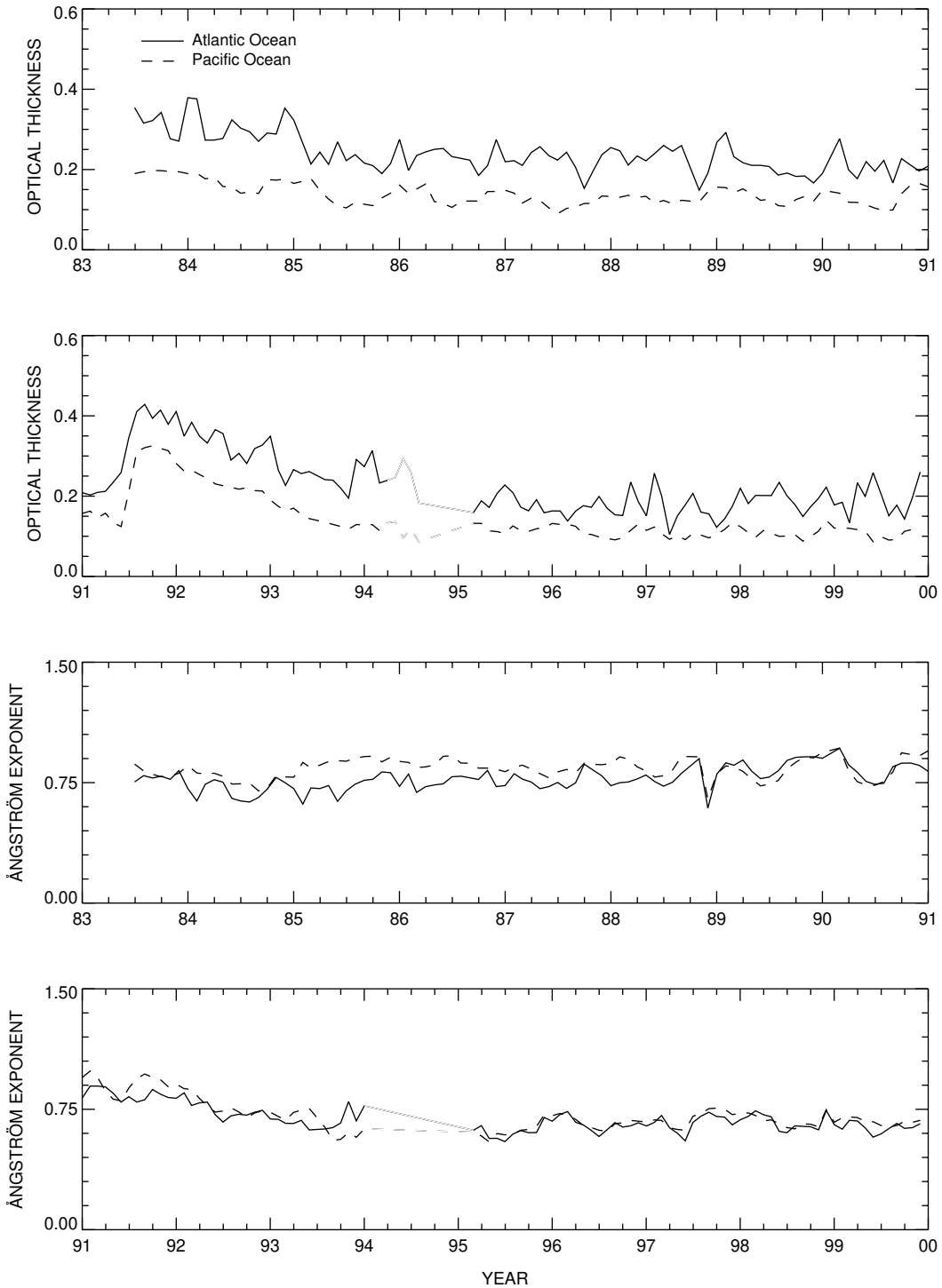

Fig. 10. Time series of monthly mean aerosol optical thickness and Ångström exponent retrieved from AVHRR data for Atlantic and Pacific Ocean areas.

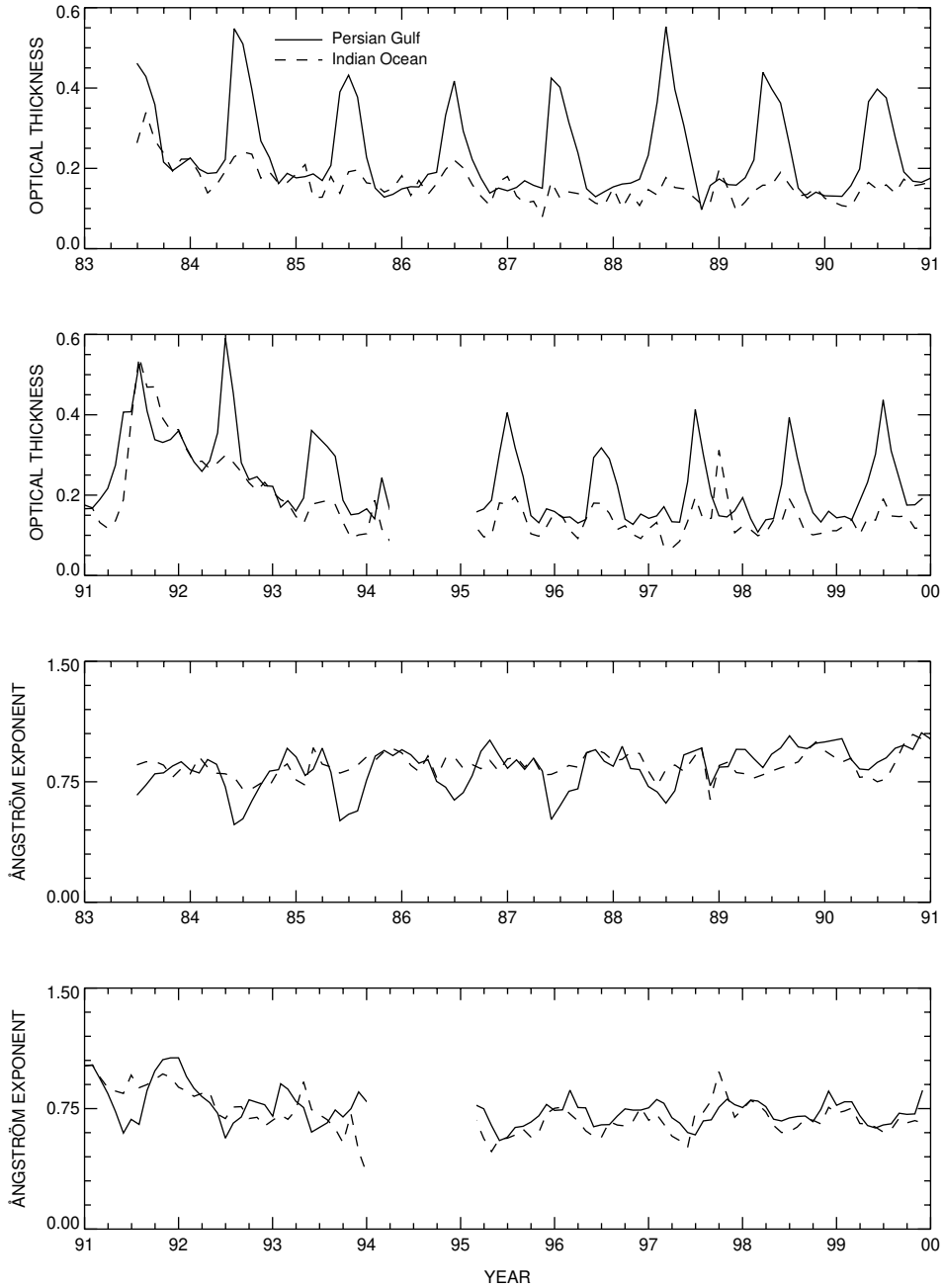

Fig. 11. Time series of monthly mean aerosol optical thickness and Ångström exponent retrieved from AVHRR radiances for Persian Gulf and Indian Ocean areas.

The time series of the optical thickness for the Persian Gulf area (Fig. 11) reveals a very strong seasonality associated with regional dust events with peak τ values exceeding 0.5. The synchronous minima in the Ångström exponent record indeed indicate the dominance of large dust particles. The adjacent Indian Ocean area is much less influenced by the dust events, exhibiting much weaker optical thickness maxima and a less obvious periodicity. A noticeable feature in the optical thickness record for this area is the maximum in the fall of 1997 caused by strong Indonesian fires. The associated peak in the Ångström exponent record indicates the presence of smaller-than-average smoke particles.

6. Conclusions

The main results of the paper can be summarized as follows.

- The use of the phase function typical of irregular mineral aerosols in the retrieval algorithm based on channel-1 AVHRR radiances indicates that the nonsphericity of dust-like and dry sea salt aerosols can lead to very large errors in the retrieved optical thickness if one mistakenly applies look-up tables based on Lorenz-Mie computations. The errors change with season and geographical location and cannot be corrected using AVHRR data alone since the latter do not provide a reliable indication of aerosol type.
- Comparisons of single-scattering albedo and Ångström exponent values generated by the operational two-channel algorithm and those measured in situ at Sable Island [11] indicate that the currently adopted value 0.003 can be a reasonable choice for the imaginary part of the aerosol refractive index in the global AVHRR retrievals.
- A discontinuity in the retrieved Ångström exponent at the time of NOAA-9 to NOAA-11 spacecraft transition and significant unexpected trends in the global mean optical thickness and Ångström exponent indicate a significant problem with post-launch calibration of channel-2 radiances from NOAA-11. This problem can, apparently, be solved using a simple re-calibration procedure to remove the observed artifacts.
- The operational two-channel retrieval algorithm was applied to the re-calibrated AVHRR radiances in order to derive a global climatology of aerosol optical thickness and size over the oceans for the period extending from July 1983 to December 1999. The global monthly mean optical thickness and Ångström exponent show no significant trends between the periods affected by major volcanic eruptions and oscillate around the average values 0.145 and 0.75, respectively. The optical thickness maxima and minima for the Southern Hemisphere occur around January–February and June–July, respectively. The Northern Hemisphere exhibits a similar pattern, but with maxima in February–April. The Northern Hemisphere mean τ systematically exceeds that averaged over the Southern Hemisphere. The results of AVHRR retrievals during the period affected by the Mt. Pinatubo eruption are consistent with the SAGE retrievals of the stratospheric aerosol optical thickness. Time series of the aerosol properties computed for four specific geographic regions show varying degrees of seasonal variability controlled by local meteorological events and/or anthropogenic activities.

Acknowledgements

We thank two anonymous reviewers for their constructive comments. This research was supported by the NASA Radiation Sciences Program managed by Donald Anderson.

References

[1] Penner JE, Charlson RJ, Hales JM, Laulainen NS, Leifer R, Novakov T, Ogren J, Radke LF, Schwartz SE, Travis L. Quantifying and minimizing uncertainty of climate forcing by anthropogenic aerosols. Bull Am Meteorol Soc 1994;75:375–400.
[2] Hansen JE, Sato M, Lacis A, Ruedy R, Tegen I, Matthews E. Perspective: climate forcings in the industrial era. Proc Natl Acad Sci 1998;95:12753–8.
[3] Kaufman YJ, Tanré D, Gordon HR, Nakajima T, editors. Passive remote sensing of tropospheric aerosol and atmospheric corrections of the aerosol effect. J Geophys Res 1997;102:16815–7217.
[4] Artaxo P, Hobbs P, Kaufman YJ, Kirchhoff, editors. Smoke, clouds, and radiation—Brazil. J Geophys Res 1998;103:31781–2137.
[5] Russell PB, Hobbs PV, Stowe LL, editors. Tropospheric aerosol radiative forcing observational experiment. J Geophys Res 1999;104:2213–319.
[6] Raes F, Bates T, editors. The second aerosol characterization experiment. Tellus 2000;52B:109–908.
[7] Mishchenko M, Penner J, Anderson D, editors. Global aerosol climatology project. J Atmos Sci 2002;59:249–783.
[8] Mishchenko MI, Geogdzhayev IV, Cairns B, Rossow WB, Lacis AA. Aerosol retrievals over the ocean by use of channels 1 and 2 AVHRR data: sensitivity analysis and preliminary results. Appl Opt 1999;38:7325–41.
[9] Geogdzhayev IV, Mishchenko MI, Rossow WB, Cairns B, Lacis AA. Global two-channel AVHRR retrievals of aerosol properties over the ocean for the period of NOAA-9 observations and preliminary retrievals using NOAA-7 and NOAA-11 data. J Atmos Sci 2002;59:262–78.
[10] Rossow WB, Schiffer RA. Advances in understanding clouds from ISCCP. Bull Am Meteorol Soc 1999;80: 2261–87.
[11] Delene DJ, Ogren JA. Variability of aerosol optical properties at four North American surface monitoring sites. J Atmos Sci 2002, in press.
[12] Nakajima T, Tanaka M, Yamano M, et al. Aerosol optical characteristics in the yellow sand events observed in May, 1982 at Nagasaki. II: Models. J Meteorol Soc Jpn 1989;67:279–91.
[13] Diner DJ, Abdou WA, Bruegge CJ, Conel JE, Crean KA, Gaitley BJ, Helmlinger MC, Kahn RA, Martonchik JV, Pilorz SH, Holben BN. MISR aerosol optical depth retrievals over southern Africa during the SAFARI-2000 dry season campaign. Geophys Res Lett 2001;28:3127–30.
[14] Dubovik O, Holben B, Eck TF, Smirnov A, Kaufman YJ, King MD, Tanré D, Slutsker I. Variability of absorption and optical properties of key aerosol types observed in worldwide locations. J Atmos Sci 2002;59:590–608.
[15] Dubovik O, Holben BN, Lapyonok T, Sinyuk A, Mishchenko MI, Yang P, Slutsker I. Non-spherical aerosol retrieval method employing light scattering by spheroids. Geophys Res Lett 2002;29(10):10.1029/2001GL014506.
[16] Pollack JB, Cuzzi JN. Scattering by nonspherical particles of size comparable to a wavelength: a new semi-empirical theory and its application to tropospheric aerosols. J Atmos Res 1980;37:868–81.
[17] von Hoyningen-Huene W, Posse P. Nonsphericity of aerosol particles and their contribution to radiative forcing. JQSRT 1997;57:651–68.
[18] Mishchenko MI, Lacis AA, Carlson BE, Travis LD. Nonsphericity of dust-like tropospheric aerosols: implications for aerosol remote sensing and climate modeling. Geophys Res Lett 1995;22:1077–80.
[19] Mishchenko MI, Travis LD, Kahn RA, West RA. Modeling phase functions for dustlike tropospheric aerosols using a shape mixture of randomly oriented polydisperse spheroids. J Geophys Res 1997;102:16831–47.
[20] Krotkov NA, Flittner DE, Krueger AJ, Kostinski A, Riley C, Rose W, Torres O. Effect of particle non-sphericity on satellite monitoring of drifting volcanic ash clouds. JQSRT 1999;63:613–30.
[21] Yang P, Liou KN, Mishchenko MI, Gao B-C. Efficient finite-difference time-domain scheme for light scattering by dielectric particles: application to aerosols. Appl Opt 2000;39:3727–37.

[22] Hovenier JW. Measuring scattering matrices of small particles at optical wavelengths. In: Mishchenko MI, Hovenier JW, Travis LD, editors. Light scattering by nonspherical particles: theory, measurements, and applications. San Diego: Academic Press, 2000. p. 355–65.
[23] Gustafson BÅS. Microwave analog to light-scattering measurements. In: Mishchenko MI, Hovenier JW, Travis LD, editors. Light scattering by nonspherical particles: theory, measurements, and applications. San Diego: Academic Press, 2000. p. 367–90.
[24] Volten H, Muñoz O, Rol E, de Haan JF, Vassen W, Hovenier JW, Muinonen K, Nousiainen T. Scattering matrices of mineral aerosol particles at 441.6 nm and 632.8 nm. J Geophys Res 2001;106:17375–401.
[25] Volten H. Light scattering by small planetary particles: an experimental study. PhD dissertation, Free University, Amsterdam, 2001.
[26] Liu L, Mishchenko MI, Hovenier JW, Volten H, Muñoz O. Scattering matrix of quartz aerosols: comparison and synthesis of laboratory and Lorenz-Mie results. JQSRT 2002 (this issue).
[27] Stowe LL, Ignatov AM, Singh RR. Development, validation, and potential enhancements to the second-generation operational aerosol product at the National Environmental Satellite, Data, and Information Service of the National Oceanic and Atmospheric Administration. J Geophys Res 1997;102:16923–34.
[28] Hansen JE, Travis LD. Light scattering in planetary atmospheres. Space Sci Rev 1974;16:527–610.
[29] Mishchenko MI, Travis LD, Lacis AA. Scattering, absorption, and emission of light by small particles. Cambridge: Cambridge University Press, 2002.
[30] Jaggard DL, Hill C, Shorthill RW, Stuart D, Glantz M, Rosswog F, Taggart B, Hammond S. Light scattering from particles of regular and irregular shape. Atmos Environ 1981;15:2511–9.
[31] Mishchenko MI, Travis LD, Macke A. Scattering of light by polydisperse, randomly oriented, finite circular cylinders. Appl Opt 1996;35:4927–40.
[32] King MD, Kaufman YJ, Menzel WP, Tanré D. Remote sensing of cloud, aerosol, and water vapor properties from the Moderate Resolution Imaging Spectrometer (MODIS). IEEE Trans Geosci Remote Sens 1992;30:2–27.
[33] Tanré D, Kaufman YJ, Herman M, Mattoo S. Remote sensing of aerosol properties over oceans using the MODIS/EOS spectral radiances. J Geophys Res 1997;102:16971–88.
[34] Kahn R, Banerjee P, McDonald D, Diner DJ. Sensitivity of multiangle imaging to aerosol optical depth and to pure-particle size distribution and composition over ocean. J Geophys Res 1998;103:32195–213.
[35] Goloub P, Tanré D, Deuzé JL, Herman M, Marchand A, Bréon F-M. Validation of the first algorithm applied for deriving the aerosol properties over the ocean using the POLDER/ADEOS measurements. IEEE Trans Geosci Remote Sens 1999;37:1586–96.
[36] Deuzé JL, Goloub P, Herman M, Marchand A, Perry G, Susana S, Tanré D. Estimate of the aerosol properties over the ocean with POLDER. J Geophys Res 2000;105:15329–46.
[37] Chowdhary J, Cairns B, Mishchenko M, Travis L. Retrieval of aerosol properties over the ocean using multispectral and multiangle photopolarimetric measurements from the Research Scanning Polarimeter. Geophys Res Lett 2001;28:243–6.
[38] Ignatov A, Stowe L. Aerosol retrievals from individual AVHRR channels. I. Retrieval algorithm and transition from Dave to 6S radiative transfer model. J Atmos Sci 2002;59:313–34.
[39] Rao CRN, Chen J. Inter-satellite calibration linkages for the visible and near-infrared channels of the Advanced Very High Resolution Radiometer on the NOAA-7, -9 and -11 spacecraft. Int J Remote Sens 1995;16:1931–42.
[40] Lacis AA, Carlson BE, Hansen JE. Retrieval of atmospheric NO_2, O_3, aerosol optical depth, effective radius and variance information from SAGE II multi-spectral extinction measurements. Appl Math Comput 2000;116:133–51.
[41] Hansen J, Sato M, Nazarenko L, Ruedy R, Lacis A, Koch D, Tegen I, Hall T, Shindell D, Stone P, Novakov T, Thomason L, Wang R, Wang Y, Jacob D, Hollandsworth S, Bishop L, Logan J, Thompson A, Solarski R, Lean J, Willson R, Levitus S, Antonov J, Rayner N, Parker D, Christy J. Climate forcings in GISS SI200 simulations. J Geophys Res 2002; 107:10.1029/2001JD001143.